Morphological descriptions using three-dimensional wavefronts

Jean Serra

August 28, 2002

Abstract

The present study deals with the analysis of three-dimensional binary objects whose structure is not obvious nor generally clearly visible. Our approach is illustrated through three examples taken from biological microscopy. In one of our examples, we need to extract the osteocytes contained in sixty confocal sections. The cells are not numerous, but are characterized by long branches, hence they will be separated using a directional wavefront.

The two other objects are more complex and will be analysed by means of a spherical wavefront. In the first case, a kidney of a rat embryo, the tissue grows like a tree, where we want to detect the branches, their extremities, and their spatial arrangement. The wavefront method enables us to define precisely branches and extremities, and gives flexible algorithms.

The last example deals with the embryonic growth of the chicken shinbone. The central part of the bone (or shaft) is structured as a series of nested cylinders following the same axis, and connected by more or less long bridges. Using wavefronts, we show that is possible to separate the cylinders and to extract, and count, the bridges that connect them.

Our presentation is completed with more theoretical results, showing the connections between geodesy, metrics and connectivity.

1 Experimental context : three-dimensional microscopy

The approach we present here was born from experience, more precisely from two separate issues in three-dimensional optical microscopy which were recently presented to me.

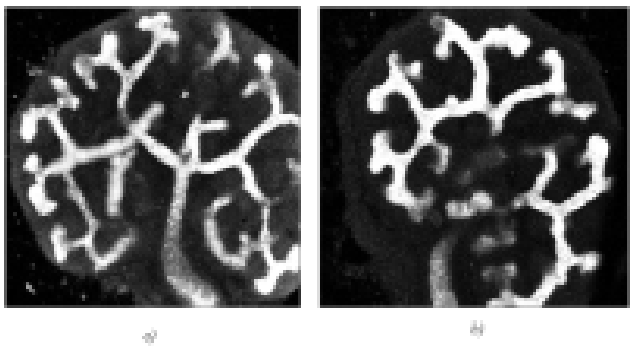

Figure 1: a) Kidney under study (supremum of the sections); b) other kidney specimen.

1.1 1st issue : the kidney

In February 1999, Dr. John BERTRAM[1], nephrologist and serving Chairman of the International Society for Stereology, spent two days at the CMM, during which he presented his current work. The subject of his research is the embryonic development of the kidney studied in animals such as the rat. He takes advantage of the property of embryonic kidney to develop in vitro, which enables him to study the organ evolution by confocal microscopy without animal destruction.[1].

Dr. Bertram proposed to work with a student from the Ecole des Mines, provided his data could be processed quantitatively. He asked more specifically our opinion on two sets of digital sections. A preliminary study, carried out during his stay, gave promising results and showed that it was possible to binarize and follow the tree from one section to another in each of the two series. Hence the decision to launch an internship [3] (Gabriel FRICOUT, 3rd year, 2000/2001), which is currently under way.

We can see in figure(1) an image of each kidney after binarization, showing that the structure develops in the form of a tree. The expected morphological description goes far beyond the preliminary study. It bears on the geometry of the tree, and involves two objects :

- extremities : where are they located ? how are they arranged in space ?
- branches : where are they located ? according to which hierarchy and length ?

Confocal microscopy results in a highly anisotropic sample. Each series contains 29 sections 30 μ thick ; in which the orientation is roughly perpendicular to the trunk.

On each section, the pixels are arranged according to a square grid, whose spacing is about 4μ. The digital volume element (voxel) looks like a cylinder

[1] Dpt of Anatomy, faculty of Medecine, Univ. de Melbourne, Parleville, Victoria 3052, Australia

with a square base, which is seven times as high as it is wide. Each branch extremity is surrounded by nephrons, whose number is indicative of the future capacity of the fully-grown kidney. The nephrons, which cannot be seen here, will become visible through a double staining. Then, we will have to study the relationship between the shape of the tree and the number of nephrons it can receive.

1.2 2nd issue : the shinbone

Dr. Staub[2] and engineer M. Mendjeli[2] study the morphogenesis of long bones, and work on the shinbones of chicken embryos. Dr. Staub designed a dynamic model of the long central zone (shaft), where the compact future bone appears as a series of nested co-axial cylinders[14](see figure2)

The experiment conducted by M. Mendjeli has consisted in slicing the shinbone shaft, perpendicularly to its axis, into a series of a hundred semi-thin sections, roughly like slicing a sausage. Their computer registration produced a matrix of data under the form of a nearly isotropic cubic grid whose step is close to the μ and whose size is approximately 300 x 300 x 100.

Unlike the previous example, the primary difficulty here is to detect the object under study. The nested cylinders are not directly visible, and one has no idea of the number of gaps and holes they may contain. However, the bone image is virtually binary. Finally, as in the preceding example, the space is "oriented" from a marker : here the central marrow space ; there, the contact zone between the kidney and the gelatine (bottom of the tree).

Is it possible to segment the concentric cylinders of the bone, and to describe them in quantitative terms (thickness, porosity, contacts between cylinders, etc ...)?

2 Method : wavefronts

2.1 Choquet's theorem

When a stone is thrown into a lake and generates a disturbance, a wave string is being created and spreads out while going around the possible obstacles, until the most remote points from the middle. The wavefront, circular in the case of a lack of borders, laps the islands and the lake contours and finally covers them completely(3).

In order to extract connected objects selected by markers, F. Meyer[9] and J.C. Klein [6] were the first ones to transfer these notions to mathematical morphology, and the very first formalization, named "geodesic metrics" was established by C. Lantuejoul and S. Beucher [7]. Indeed, in figure 3, the zone of the reference set Z, swept between instants 0 et λ by the wavefront born from point x at the original instant is a disk $B_\lambda(x)$, smaller than the Euclidean

[2] Laboratoire de recherches orthopédiques - CHU Lariboisière - St Louis - 75010 Paris

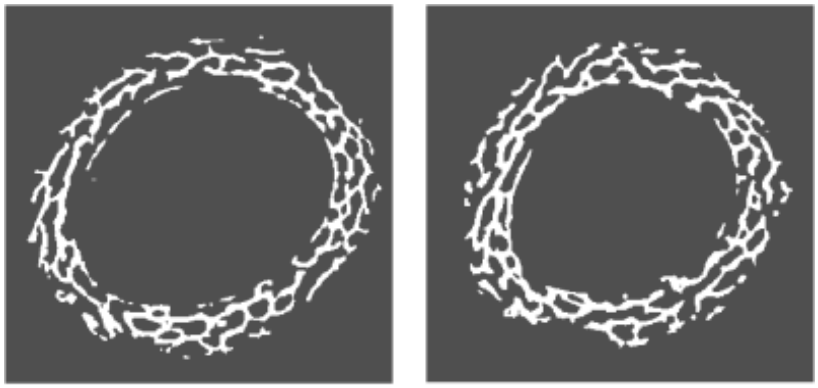

Figure 2: Two horizontal sections of a shinbone epiphysis

Figure 3: a) Geodesic disc ; b) Geodesic distance function in two dimensions

disk with a radius λ and completely containd in Z. When the reference set Z is compact, the induced metrics $\{B_\lambda(x), x \in Z\}$ satisfy the following theorem, from G. Choquet ([2],theorem 11-6)

Theorem 1 *Let E be a metric compact space and let A et B be two disjoint closed subsets of E. If there exist rectifiable curves with extremities in A and B respectively, and if λ stands for the lower limit of their lengths, then there exists a simple arc whose length is λ and whose extremities lie in A and B respectively.*

In what follows, we will always suppose that reference sets Z are compact, and that for any points x, y selected in a same connected component Z, there is a rectifiable path with a length limited by a $\lambda_{\max}(Z, x)$ and linking these two points. This happens, particularly, when in $\mathbb{R}^n$, the set Z is the topological closure of a bounded open set. Rectifiable arcs, as a precaution, are meant to exclude compact sets such as, for instance, a spiral which winds indefinitely around a circle.

2.2 The ultimate elements of the wavefronts

This section takes up C. Lantuejoul's and S. Beucher's results [7], but presents them differently. When using geodesics, it becomes possible to associate any point $x \in Z, Z \in \mathbb{R}^n$, with the point or points $y \in Z$ which are the furthest away from x. Indeed, let $\overset{\circ}{B}(\lambda, x)$ be the geodesic open ball of radius λ and centre x, and $\lambda_0$be the upper limit of the λ such that $\overset{\circ}{B}(\lambda, x)$ be strictly contained in Z. As the non empty compact sets $\left\{ Z \backslash \overset{\circ}{B}(\lambda, x), \lambda < \lambda_0 \right\}$ decrease and that $\mathbb{R}^n$ is a separated space, the intersection

$$\bigcap_{x<\lambda_0} \left[Z \setminus \overset{\circ}{B}(\lambda, x) \right] \tag{1}$$

is itself a non empty compact set, whose points are all at the maximum distance λ_0 from x. This intersection is named "geodesic ultimate eroded set", and $\overset{\circ}{B}(\lambda_0, x)$ is the "geodesic ultimate dilated set" of point x.

The existence of extreme points may also be considered in a regional framework, and not a global one anymore. We must suppose that, Z and x being given, it is possible to find a $\mu(Z, x) \leq \lambda_0(Z, x)$ such that each connected component of $Z \setminus \overset{\circ}{B}(\lambda, x), \mu \leqslant \lambda \leqslant \lambda_0$ decreases without subdividing. Then, the previous analysis should simply be applied to sets

$$K_i \cap \left[Z \setminus \overset{\circ}{B}(\lambda, x) \right] \qquad \mu \leqslant \lambda \leqslant \lambda_0$$

where the $K_i, i \in I$ refers to the connected components of $Z \setminus \overset{\circ}{B}(\mu, x)$. Therefore, we obtain the farthest connected components from point x, such as, for instance, the fingers tips for x taken around the middle of the wrist.

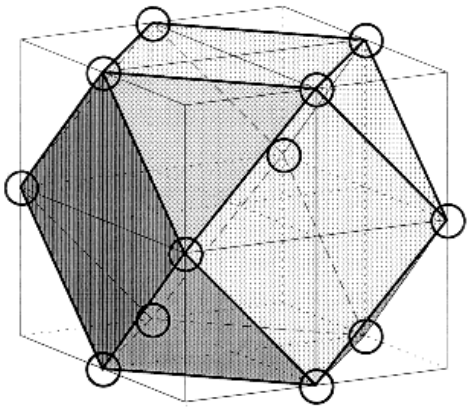

Figure 4: Cube-octahedron

Both algorithm families about geodesics correspond to both our points of view. Invasion by geodesic balls led to all the particles reconstruction variants (deletion of the grains crossing the field border, hole filling, individual analysis, etc ...) and the search for extreme residues led to the ultimate eroded points, to the objects limits and to the length of a connected component (as a supremum of the distances between pairs of extreme points).

2.3 Digitization

The digitization of geodesic operations may cause errors, but limited ones ; indeed, it is advisable to choose, as a circle or unit sphere, the closest shapes to their Euclidean homologues. Therefore, in 2D the hexagon, whose six vertices are equidistant from the center is better than the square, and, for the same reason, the cube-octahedron is better than the cube in 3D.

This $\mathbb{Z}^3$ ball is very easy to build, when a numerical data network in square grid is available[13]. It suffices to shift all even planes by half a diagonal of the unit cube (any diagonal, but always the same one). In practice, data are of course not moved, but only structuring elements. For example, the substitute for the 13 vertices of the regular cube-octahedron (4) is calculated by dilating the central point according to the staggered unit cube-octahedron presented in figure(5). It requires three successive planes and differs whether the center lies in an even plane or in an odd one.

The wavefront emanating from this central point starts with the point 12 neighbours ; when the interplane equals $a/\sqrt{2}$ (a = square grid spacing of the horizontal planes), the structure becomes completly isotropic and the 12 neighbours are equidistant from the center. This will be our assumption (section 5) about the shinbone, but this hypothesis is not essential, and, in any case, cannot be ventured for the study about embryonic kidneys (section 3)

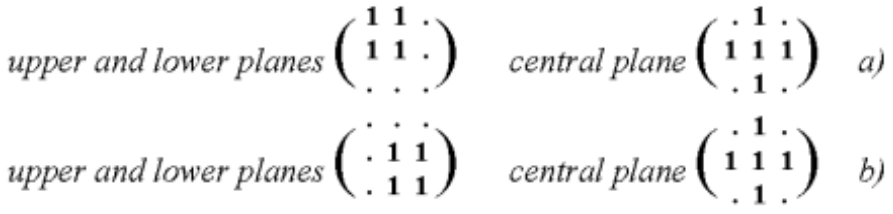

Figure 5: Staggered successive planes, for simulating a cube-octahedron on a cubic grid

The switch from the unit ball $C(x)$ of $\mathbb{Z}^3$ (octahedron, prism or cube) to its geodesic version $B_1(x)$ inside a mask Z is

$$B_1(x) = C(x) \cap Z$$

and the geodesic ball $B_x(x)$ of the size is obtained by n iterations of the previous one :

$$B_n(x) = B_1[B_{n-1}(x)] \cap Z$$

The corresponding wavefront, or geodesic *sphere* equals

$$F_n(x) = B_{n+1}(x) \setminus B_n(x)$$

2.4 Wavefronts and tree diagrams

Let Z be a compact set in $\mathbb{R}^n$ and $x \in Z$, be a point in Z. We propose to study the evolution of the connected components number of the wavefront $F(\lambda, x)$ when, as λ increases, the compact space Z is swept. The two types of branching, division or confluence, supposedly remain in finite number when $\lambda \in [0, \lambda_{\max}]$, so that for any branching at $\lambda = \lambda_0 < \lambda_{\max}$, it is always possible to find an open interval $]\lambda_1, \lambda_2[$ containing λ_0, and inside which there are no other branching. The number of branches which may gather in λ_0 is supposed to be finite. Finally, as the branching may take the two dual shapes (division or confluence) when λ increases, it is conventionally agreed in the proof below that the passage $\lambda_1 \to \lambda_2$ corresponds to a division

Therefore, we are led to the situation described in figure (6), where point x is in black, the ball $\overset{\circ}{B}(\lambda_0, x)$ in light grey, its complement $K(\lambda_0)$ in Z in dark grey, and where the white wavefront indicates the precise moment of the branching. So, the compact set

$$K(\lambda) = Z \setminus \overset{\circ}{B}(\lambda, x)$$

has a unique connected component, when $\lambda < \lambda_0$, and more when $\lambda > \lambda_0$. In order to determine what happens when $\lambda = \lambda_0$, we first observe that for compact sets, we have $\cap \{K(\lambda), \lambda < \lambda_0\} = K(\lambda_0)$.

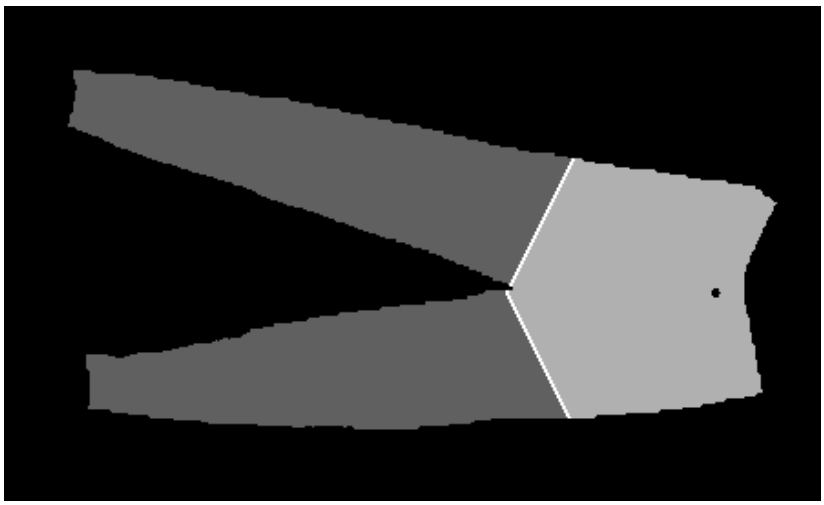

Figure 6: Example of branching

The compact $K(\lambda_0)$ is composed of only one connected component. Otherwise, they would be separated by a minimum distance d ; but this is incompatible with the fact that, for any dilation of size ε, with $0 < \varepsilon < d$, the geodesic dilate of $K(\lambda_0)$ becomes connected. Therefore, the front $F(\lambda_0, x)$ itself is connected, as otherwise, to switch from one of its components to another one, it would be necessary to cross a $K(\lambda)$ with $\lambda > \lambda_0$, but these $K(\lambda)$ are not connected anymore.

When Z has several branchings, the same description applies for each branch, upwards or downwards from the propagation from point x, which consequently partitions the set Z into a series of successive pieces.

The case of the X branching has also to be considered. It occurs when at least two branches stop at the critical front, and at least two of them start from there. In this case, the intermediary connected region is reduced to the front in λ_0, for, if it was larger, we would come back to the previous case; and if the front was not taken into accout, we would no longer have a critical element, but only separated branches. By gathering these results, we can state :

Proposition 2 *Let Z be a compact of $\mathbb{R}^n$. If, for any point $x \in Z$, the wavefront $F(\lambda, x)$ emanating from x admits a finite number of connected components, with a finite variation, then, as radius λ varies, $F(\lambda, x)$ partitions Z into a finite number of connected sections, corresponding to open intervals of λ, and separated by connected components of the front which are located at the critical points of the branchings.*

Clearly, the mapping $x \to P(x)$ which associates with any point $x \in Z$ the tree diagram characterized by the proposition, depends on the choice of point x,

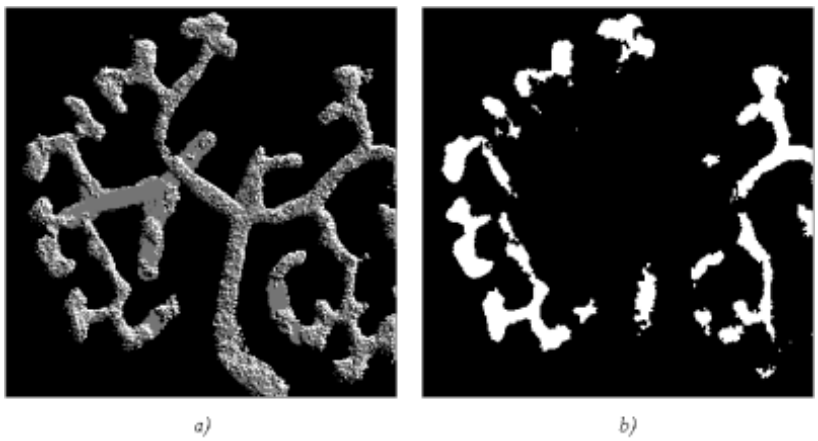

Figure 7: a) Perspective view of the binarized kidney; b) confocal section n°14

even if, when considering the common meaning of a tree, the partition remains almost the same for all the points selected low enough in the trunk. Besides, in this case, the tree may be defined as a partition for which there is no confluence for a suitably selected origin x (i.e. in the trunk).

Note that we are talking about connectivity here, and not about homotopy: in $\mathbb{R}^3$ particularly, the sections may show closed pores or toric holes.

3 Use of the tree diagram for embryonic kidneys

In order to illustrate the above matter, we propose to segment the first one of the two kidneys of1. The analysis contains four steps :

1/ set construction from the initial data ;
2/ geodesic distance function of a marker in the set;
3/ extremities;
4/ branches.

3.1 Binarization

This simple operation only requires a thresholding between 60 and 255, followed with the fill-in of the bi-dimensional internal pores. Still, the main connected component has to be extracted. In order to do this, we take as marker x one point at the beginning of the trunk. The reconstruction shows that the kidney tree diagram is broken around the middle in two separated parts. This is caused by the inaccuracy of confocal microscopy. In order to put it right, both parts have been reconnected by a small closing, as shown in figure(7a).

Figure 8: Geodesic distance function from the anchorage point (negative view of the supremum of the sections)

3.2 geodesic distance function

The geodesic distance function starts from marker x at the base of the kidney and progresses inside the tree according to unit cube-octahedra (see figure (8))

3.3 Extremities

The extremities are nothing but the region maxima of the previous geodesic function. These ultimate eroded points are shown on figure(9a), where lots of quite unsignificant but very small real maxima can been observed. They are removed by a small surface opening (figure(9)b). When using this algorithm in routine, we would better start with a regularization of the set under study by means of an isotropic tridimensional opening of size 1 or 2, providing that it does not break the connectivity.

3.4 Branchings

The extraction of branchings, which is conceptually simple, may lead nevertheless to a consequent computing time. Considering the quite visible structure of the projected tree, the algorithm used below is slightly less precise, but faster an easier to implement.

In a first step, bidimensional branchings on the tree projection are investigated, then, we get back to the 3D space by building vertical cylinders whose bases are located at the 2D branchings, and slightly dilated (size 2). Finally, we take the intersection between these cylinders and the 3D tree. The operation leads to figure(10).

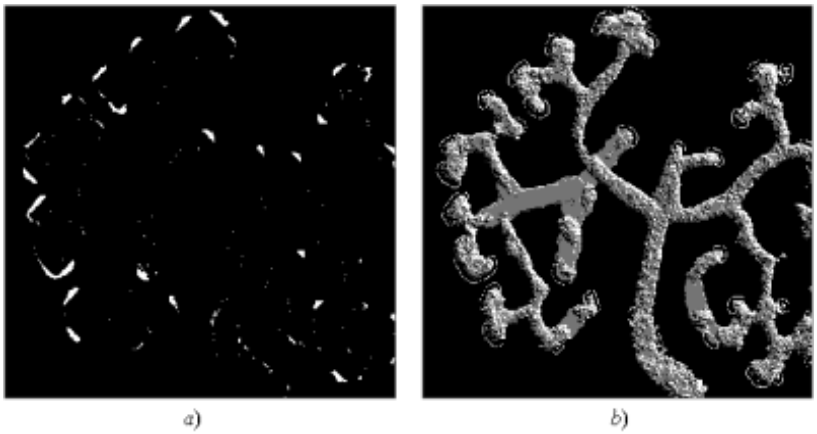

Figure 9: a) All extremities of the Kidney ; b) Filtered extremities.

Figure 10: Projection of the 3D branchings

3.5 Results

In all, starting from the connected kidney tree, we got to its segmentation into disjoint branches separated by thin branchings. Some branches contain one or more, of the tree extremities. From such a segmentation, it beomes now possibleto replace the object under study by a "tree" in the meaning of graph theory, where the edges can be weighted geometrical characteristics (volume, length, location of its center, possible end points ... etc).

4 Euler-Poincaré number and space graphs

Historically, the Euler-Poincaré constant (in brief:EPC) appeared in two slightly different domains of mathematics. Firstly, there was Euler's reasoning about the relations between the polyhedrons vertices, edges and faces, which was formalized in terms of planar graphs by Cauchy. This way of thinking leads to counting algorithms, which are based on the elementary edges, squares and triangles (in the hexagonal grid). It extends to various cubic, cube-octahedron and rhombo-dodecahedron of $\mathbb{R}^3$, without any particular theoretical difficulty, but with a growing heaviness of the elementary operations to be carried out.

The second way, Poincaré's, and Hadwiger's later on, links the successive definitions of EPC thanks to an induction holding on the dimensions of the space [5]. When transposed to a digital grid, this approach is limited to cubic (or to parallelepipedic) grids, but, in return, leads to a much simpler and faster expression than the graphs one. Thus, for a bounded digital set A, we have :

In $\mathbb{Z}^1$, $v_1(A) = N(\text{vertices}) - N(\text{edges}) = N(\bullet) - N(-)$

In $\mathbb{Z}^2$, for the square grid :

$$\begin{aligned} v_2(A) &= N(\text{vertices}) - N(\text{edges}) + N(\text{faces}) \\ &= N(\bullet) - N(-) - N(|) + N(\square) \end{aligned}$$

Still in $\mathbb{Z}^2$, if we agree on calling $N_1(A)$ the sum of the constants $\overline{\nu_1}$ of the horizontal sections of A, we can see that

$$v_2(A) = \overline{\nu_1}(A) - \overline{\nu_1}(A \ominus |),$$

where $A \ominus |$ stands for the Minkowski substraction of A by the unit vertical segment.

In $\mathbb{Z}^3$, this is the same, and Euler's number $v_3(A)$ defined as

$$v_3(A) = N(\text{vertices}) - N(\text{edges}) + N(\text{faces}) - N(\text{blocks})$$

is expressed by the same increment as before, for

$$v_3(A) = \overline{v_2}(A) - \overline{v_2}(A \ominus |) \tag{2}$$

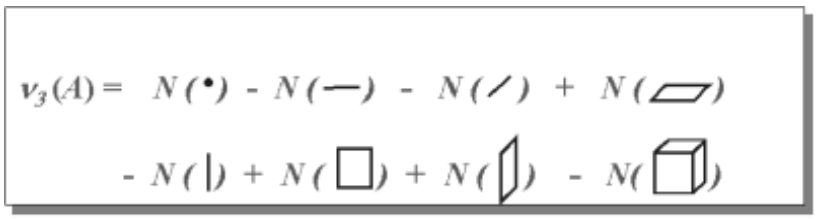

Figure 11: Euler-Poincaré Constant in $\mathbb{R}^3$

when $\overline{v_2}(A)$ is the sum of Euler bidimensional numbers of the horizontal sections of A, and where $\ominus$ stands for he Minkowski substraction of A by the unit vertical segment (equation (2) can easily be extended to $\mathbb{R}^n$ by recurrence). Constant v_3 is independent of the choice of the "vertical" direction.

From an experimental point of view, the equation (2) is very convenient, for in image processing systems, Euler bidimensional constants are generally rapid to get and the unit linear erosion between two consecutive planes is a simple operation too. It is this equation (2) that has been implemented in the shinbone example below.

Finally, remember that the EPC of a simply connected object (i.e. homeomorphic to a cube) equals 1, that of a torus (typically, a donut) equals 0, and that of spherical crown (such as a football) equals 2. Moreover, the constant v is C-additive, which means that

$$v(A) + v(A') = v(A \cup A') + v(A \cap A'),$$

an equation that allows one to reduce complex figures to the most simple ones. Thus, the ECPC of lampshade pierced by 1000 pin holes equals -1000.

5 Shaft of chicken embryo shinbones

5.1 Purpose

The bone zone under study is situated in the central part of a chicken embryo shinbone, whose axis defines the vertical.The experimental data form a series of 98 rectangular slices of 320 x 310 pixels each. The uniform grey of the shinbone phase allowing an easy threshold (see12a), the two problems to be solved are then the following :

1/ Implementing and checking Dr Staub's model, that is to say switching from the model of nested cylinders to an effective segmentation of the bone into nested structures thanks to some convenient quantitative criterion (to be found);

2/ Once the segmentation is achieved, extracting more specifically the bridges that link two successive cylinders, and calculating the homotopy of both bridges and cylinders.

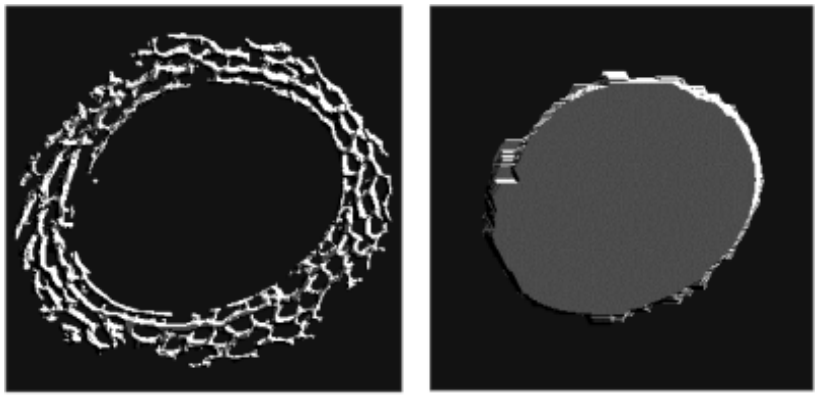

Figure 12: a) perspective view of bone1; b)Central cylindric marker M

5.2 Algorithm

For the sake of pedagogy, we work, on the one hand, on all 98 slices, and on the other hand, on the first 14 ones only. We call "bone" the first file, and "bone1" the second one. Thanks to reduced thickness file bone1, some structures are made more easily visible; moreover, the comparison between the wavefronts of bone and bone1 will inform us about the representativity of sample bone1.

If the nested cylinders model is correct, the wavefront stemming from the central medulla zone and penetrating into the bone should propagate more rapidly when it floods a cylindrical crown than when it crosses the narrow isthmuses that link the crowns altogether. Therefore, we have to :
- generate a relevant central marker M;
- plot the curve of the wavefront surface $F(\lambda, M)$ versus distance λ, which should show oscillations with more or less periodic minima ;
- decompose the geodesic wave into sections limited by minima values (bone segmentation);
- extract the wavefront at each minimum, which will result into bridges;
- calculate Euler constant for bridge sets, and cylinders;

... all operations that will now be executed.

5.3 Results

The central marker M is obtained by working one section after the other, and by extracting the central pore after opening (algorithm bone1), see12b

The measurement variation of the wavefront surface, for both files bone and bone1 is plotted in figure(13). Their minima are approximately on the same abcissae, for instance 16 instead of 13 or 6 instead of 5, which is an auspicious

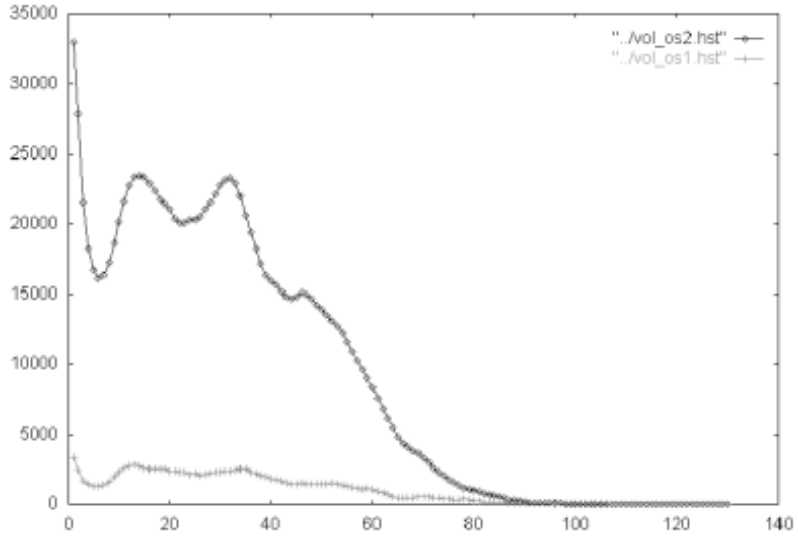

Figure 13: Plot of the wavefront surface versus the propagation steps

start.

Bone and bone1 segmentations, carried out from the following minima abcissae

$$6; 22; 44; \ldots\ldots\ldots\ldots \text{ for bone}$$
$$5; 18, 24; 41, 65; \ldots\ldots\ldots\ldots \text{ for bone1}$$

lead to the results shown in figure (14).

In order to extract the branchings between cylinders, a stronger and partially false hypothesis has to be made: the wavefronts corresponding to each minimum of the plot are supposed to be exclusively located in these narrows. Based on this approximation, the bridges between cylinders n°i and $i+1$ match with the set difference between the m + 1 and m sized-geodesic dilates, where m is the abcissa of a minimum. The contact zones between the first two cylinders, for both files bone and bone1are displayed on figure (15).

We now treat the last point, about countings on the various extracted sets. As one can note on the following table, the bone is quite pierced and broken.

Region	*Euler Poincaré number*	
	bone	*bone1*
initial bone	*- 1 536*	*- 237*
connected component, adjacent to the marker	*- 1 885*	*- 275*
bridges between the first two cylinders	*1 447*	*205*
same bridges, followed by a unit dilation	*32*	*10*

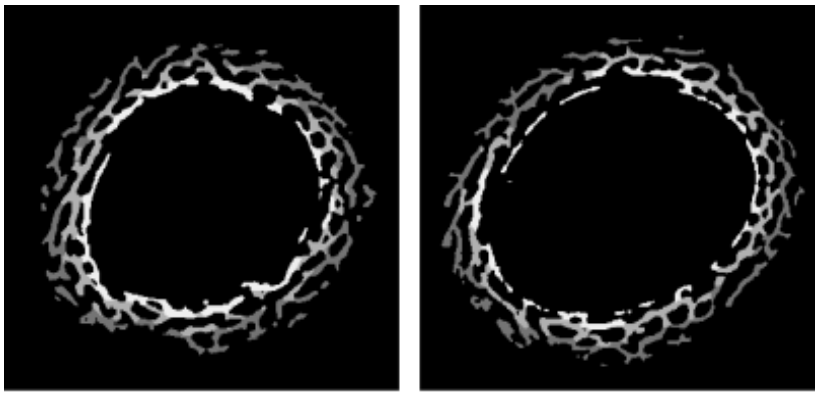

Figure 14: 3D segmentations of two slices.

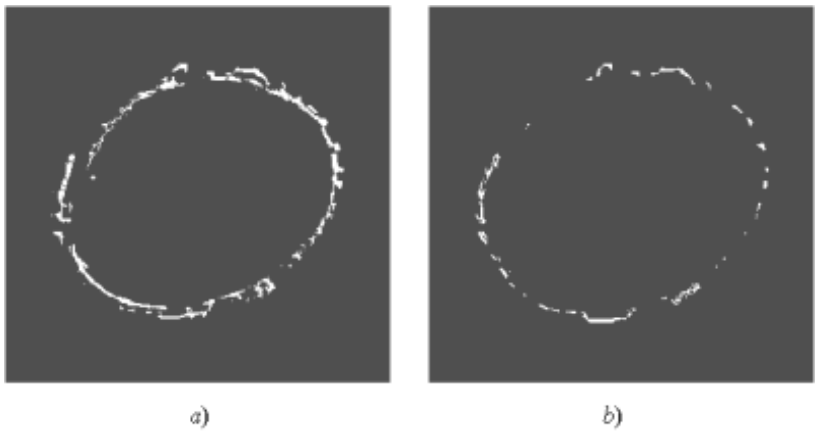

Figure 15: Perspective views of the dilated bridges, for "bone" and "bone 1"

Broken, for when reducing the object to its part adjacent to the central marker, at least 1885 - 1 536 = 349 small isolated parts are removed (experimental artifacts?). Pierced, for this main connected component has 1885 holes, if it is admitted that it does not contains internal closed pores (this seems realistic when we consider the thicknesses).

The EPC of the bridges (1447) seems quite high. In fact, more than a nut linking one cylinder to the following one, a joint rather looks like a bundle of fine fibers. This is the reason why an elementary dilation (the 13 voxels of the unit cube-octahedron brings Euler-Poincaré number 1 447 down to 32.

6 Metrics and dilation

In both examples, we decided to start from digital metrics, those whose balls are the cube-octahedron of $\mathbb{Z}^3$. Then, we considered the cube-octahedra $\mathrm{B}_1(x)$ centered in $x, \in \mathbb{Z}^3$, and with a size 1 as the structuring elements, and we have used their successive iterations to generate the wavefronts. Finally, we have considered the wavefronts as the spheres in a new metric, named geodesics, thanks to the Choquet theorem.

Meanwhile, we have approximated sets and Euclidean operators with finite representations: neither the kidney, nor a mammal bone can be reduced to some points on a square lattice. But we have also surreptitiously replaced the metric balls with a set of dilations when time came to implement the first ones. Are these two notions equivalent ? More generally, to what extent does a dilation family $\{\delta_\lambda, \lambda > O\}$ on a lattice $\mathcal{L}$ generate metrics on $\mathcal{L}$? Is it sufficient that the δ_λ increase with the positive parameter λ ? This is what we are going to study now.

In a first step, we will compare the dilations to ecarts rather than to distances. First, because it is more simple, and second because the notion of an ecart better suits the lattice structure.Following G. Choquet ([2],p. 61)

Definition 3 *We call an ecart on a set $\mathcal{L}$ any mapping of $\mathcal{L} \otimes \mathcal{L}$ in $\overline{\mathbb{R}}_+$ such that*

i/ $(x = y) \Longrightarrow (e(x, y) = 0)$
ii/ $e(x, y) = e(y, x)$
iii/ $e(x, y) \leqslant e(x, z) + e(z, y)$

The two differences with the notion of a distance, namely that the ecart e may equal $+\infty$ and that two distinct points may have a zero ecart, are essential to structure the ecarts into complete lattices, which is impossible to do with distances. Actually, let $e(x, y) = \sup\{e_j(x, y), j \in J\}$, when the e_j are ecarts. Clearly, mapping $e : \mathcal{L} \otimes \mathcal{L} \to \overline{\mathbb{R}}_+$ satisfies both axioms *i/* and *ii/*.

On the other hand, we have for any i

$$e_i(x, y) \leqslant e_i(x, z) + e_i(z, y) \leqslant e(u, z) + e(z, y)$$

that implies

$$e(x,y) \leqslant e(x,z) + e(z,y)$$

Therefore, the supremum of ecarts is n ecart. Moreover, there is a smaller ecart $e(x,y) = 0, \quad \forall x, y$; as any sup half lattice with a minimal element is a complete lattice, we can say

Proposition 4 *The class of ecarts $e : \mathcal{L} \otimes \mathcal{L} \to \overline{\mathbb{R}}_+$ on a space $\mathcal{L}$ is a complete lattice where the supremum coincides with the numerical supremum.*

The links between ecarts and dilations are governed by the following result

Proposition 5 *Let $\mathcal{L}$ be a complete lattice and $\{\delta_\lambda, \lambda > 0\}$ be a family of dilations from $\mathcal{L}$ into itself, depending on a positive parameter λ. The δ_λ generate an ecart on $\mathcal{L}$ if and only if*

$$iv/ \quad \delta_\lambda \geqslant I \qquad (\ \delta_\lambda \ \textit{is extensive for any } \lambda \geqslant 0)$$

$$v/ \quad \delta_\lambda \delta_\mu \leqslant \delta_{\lambda+\mu} \qquad \lambda, \mu \geqslant 0 \tag{3}$$

Then, the family δ_λ is increasing in λ and the quantity

$$e(x,y) = \inf \lambda \{x \leqslant \delta_\lambda(y), y \leqslant \delta_\lambda(x)\} \qquad x, y \in \mathcal{L} \tag{4}$$

defines an ecart on the lattice $\mathcal{L}$.

Proof. The two axioms $iv/$ et $v/$ imply the increasingness of the application $\lambda \to \delta_\lambda$, as, for any μ and any λ, we get

$$I \leqslant \delta_\lambda \Longrightarrow \delta_\mu \leqslant \delta_\mu \delta_\lambda \leqslant \delta_{\mu+\lambda}.$$

Let us prove that they also imply the three axioms of an ecart. As $x \leqslant \delta_\lambda(x)$ for any λ (axiom $iv/$), the quantity $e(x,x) = 0$ for all x (axiom $i/$) ; the axiom $ii/$ results from the symmetry of the inequality 3. In order to verify the triangular inequality $iii/$, let us consider three elements x, y, z of $\mathcal{L}$ with $\lambda_1 = e(y,z), \lambda_2 = e(z,x), \lambda_3 = e(x,y)$.

If λ_1 or $\lambda_3 = \infty$, then $\lambda_2 \leqslant \lambda_1 + \lambda_3$. If not, from the inequalities

$$x \leqslant \delta_{\lambda 3+\varepsilon}(y) \qquad \textit{and} \qquad y \leqslant \delta_{\lambda 3+\varepsilon}(x)$$

for any $\varepsilon > 0$, and from

$$y \leqslant \delta_{\lambda 1+\varepsilon}(z) \qquad \textit{and} \qquad z \leqslant \delta_{\lambda 1+\varepsilon}(y)$$

we draw by application of axiom $v/$ that

$$x \leqslant \delta_{\lambda 3+\varepsilon} \delta_{\lambda 1+\varepsilon}(z) \leqslant \delta_{\lambda 1+\lambda 3+2\varepsilon}(z)$$

and similarly that $z \leqslant \delta_{\lambda 1+\lambda 3+2\varepsilon}(x)$. Therefore,

$$\lambda_2 \leqslant \lambda_1 + \lambda_3 + 2\varepsilon$$

for any $\varepsilon > 0$, which implies the triangular inequality.

Conversely, start from an ecart e on $\mathcal{L}$ of closed balls δ_λ

$$\delta_\lambda(x) = \{y : e(x,y) \leqslant \lambda\} \tag{5}$$

Axiom $i/$ implies that the δ_λ are extensive (axiom $iv/$). In order to prove axiom $v/$ note that for any element $z \leqslant \delta_\lambda\delta_\mu(x)$, there is an element $y \leqslant \delta_\mu(x)$ with $z \leqslant \delta_\lambda(y)$, i.e.

$$e(x,y) \leqslant \mu \qquad \text{and} \qquad e(y,z) \leqslant \lambda$$

which implies, by triangular inequality $iii/$

$$e(x,z) \leqslant e(x,y) + e(y,z) \leqslant \lambda + \mu$$

therefore $z \leqslant \delta_{\lambda+\mu}(x)$ and finally

$$\delta_\lambda\delta_\mu(x) = \bigvee\{z : z \leqslant \delta_\lambda\delta_\mu(x)\} \leqslant \delta_{\lambda+\mu}(x)$$

which is axiom $v/$ ■

It results from the proposition that both equations 4 and 5 joining ecart and dilation are equivalent and reciprocal.

6.1 Distances

When considering distances, things become a bit more complicated. Firstly, we have to limit ourselves to those families of elements of $\mathcal{L} \otimes \mathcal{L}$ which admit *finite* ecarts (a class which does not need to be a sub-lattice of $\mathcal{L}$), and, furthermore, the extensivity axiom $iv/$ is not enough to guarantee axiom $i\prime/$

$$i\prime/\ (x = y) \Longleftrightarrow (d(x,y) = 0) \tag{6}$$

For instance, if we consider the family

$$\begin{aligned} \delta_\lambda(x) &= \{x, x_o, y_o\} \qquad \lambda > 0 \\ \delta_o(x) &= \{x\} \end{aligned}$$

where x_o and y_o are two fixed and distinct elements of $\mathcal{L}$, then proposition5 applies : we do have an ecart, but no distance, for $e(x_o, y_o) = 0$ whereas $x_o \neq y_o$. The simple extensivity $iv/$ has to be replaced by the axiom $iv\prime/$ of monotonous convergence:

$$iv\prime/\ \lambda \downarrow 0 \Longrightarrow \delta_\lambda \downarrow I$$

which is a lot more severe (it means that the δ_λ increase with λ and that $I = \bigwedge\{\delta_\lambda, \lambda > 0\}$). When this condition is satisfied, then $d(x,y) = 0$ implies, according to the equation 4 that

$$x \leqslant \bigwedge\{\delta_\lambda(y), \lambda > 0\} = y$$

and, as well, that $y \leqslant x$. Conversely, the counter-example just presented with (x_o, y_o) proves that the condition is necessary. Therefore, we can state:

Proposition 6 *Let $\{\delta_\lambda, \lambda > 0\}$ be a family of dilations of lattice $\mathcal{L}$ into itself. The δ_λ generate a metrics if and only if*

$$iv\prime/\lambda \downarrow 0 \;\; implies \;\; \delta_\lambda \downarrow I$$
$$v/\delta_\lambda \delta_\mu \leqslant \delta_{\lambda+\mu}$$

and if its domain is restricted to the classes $\mathcal{L}$' of elements of $\mathcal{L}$ such that, for any $x, y \in \mathcal{L}'$ we get

$$d(x,y) = \inf\{\lambda : x \leqslant \delta_\lambda(y), y \leqslant \delta_\lambda(x)\} < \infty \tag{7}$$

when d is the ecart induced on $\mathcal{L} \otimes \mathcal{L}$ by the δ_λ.

The Hausdorff ecart on $\mathcal{P}(\mathbb{R}^n)$, which becomes a distance when restricted to the non-empty compact sets of $\mathbb{R}^n$ perfectly illustrates the distinction between propositions5and6. In addition it shows how, when applied to a lattice such as $\mathcal{P}(E)$, the Hausdorff type equation 7 leads to a ecart on E if restricted to the singletons of $\mathcal{P}(E)$.

The ball $B_\lambda(x)$, with a radius λ and centered in x is easily expressed if we introduce the dilation $\overset{\vee}{\delta}$ *reciprocal* of δ, and defined by the equivalence

$$x \leqslant \delta(y) \Longleftrightarrow y \leqslant \overset{\vee}{\delta}(x)$$

Whether ecart or distance are concerned, considering the equations 4 and 7, we get,

$$B_\lambda(x) = \{y : d(x,y) \leqslant \lambda\} = \left[\bigwedge_{\mu>\lambda} \delta_\mu(x)\right] \wedge \left[\bigwedge_{\mu>\lambda} \overset{\vee}{\delta}_\mu(x)\right] \tag{8}$$

When δ_λ is $\downarrow$-continuous for any λ, the equation is reduced to

$$B_\lambda(x) = \delta_\lambda(x) \wedge \overset{\vee}{\delta}_\lambda(x)$$

Finally, if the dilation is symmetrical, i.e. is equal to its transpose, we finally get $B_\lambda = \delta_\lambda$. This is the case, for instance, when the δ_λ are homothetic of a symmetrical convex set. In $\mathcal{P}(\mathbb{R}^n)$, G.Matheron [8] proved that if the δ_λ commute under translations, and therefore, express Minkowski additions, they satisfy an additive semigroup of a positive parameter, i.e.$\delta_\lambda \delta_\mu = \delta_{\lambda+\mu}$ if and only if the δ_λ are homothetic and symmetrical convex sets (it is easy to prove that magnification implies $\delta_\lambda \delta_\mu \geqslant \delta_{\lambda+\mu}$, which finally leads to the equality $\delta_\lambda \delta_\mu = \delta_{\lambda+\mu}$, but the converse proposition is less obvious).

7 Connectivity, geodesics and semigroup

For being able to build wavefronts, the data of a prior metric is a necessary but insufficient condition. We must also make sure that any point of the space remains accessible from any other one by a series of arbitrary small dilations, namely, in the digital case, of the unit size. Expressed in terms of distance, this condition leads to the concept of a well linked metric space (([2], p 76).

Definition 7 *a metric space E is well linked if, for any pair (a,b) of points in E and for any $\varepsilon > 0$, there is a finite sequence of points in E : $a_1 ... a_n$, with $a_1 = a$ and $a_n = b$ so that $d(a_i, a_{i+1}) \leq \varepsilon$ for any $i < n$.*

Such a definition allows one to interpret the *connectivity notions* in terms of metrics. In fact :

Proposition 8 *For a compact metrical space, the properties of being connected (in the sense of topological connectivity), and being well linked are equivalent ([2], p 77)*

Proposition 8 validates the geodesic extraction procedures of connected components and gives a Euclidean meaning to these digital approaches ([11], p 82), if and only if the underlying metrics are well linked.

Intuitively, we see that non well linked metric contains some kind of vertical walls of distances, more or less long and thick, and placed in the space. For instance, in the Euclidean plane of co-ordinates of x and y, the sum d of the Euclidean distance d_1, plus the following ecart d_2

$$\begin{array}{ll} d_2\left[(x,y)\,(x',y')\right] = 0 & \text{if } x \text{ and } x'<0 \text{ or if } x \text{ and } x' \geq 0 \\ d_2\left[(x,y)\,(x',y')\right] = 1 & \text{otherwise} \end{array}$$

is still a distance, as the sum of a distance and of a bounded ecart, but it does not allow one to cross the ordinates axis with dilations smaller than 1.

Choquet poposition n°8 links the connectivity of a compact set with a metric characteristic about *paths*. However, image processing brings into play the dual point of view. It uses the wavefronts which emanate from this point, but without paying attention to the corresponding radius. The following proposition allows one to pass from one point of view to the other :

Proposition 9 *Let $\{\delta_\lambda, \lambda > 0\}$ be a family of symmetrical dilations from lattice $\mathcal{L}$ into itself, which generate a metric on $\mathcal{L}$. This metric admits geodesics if any only if the δ_λ satisfy the semi group of law*

$$\delta_{\lambda+\mu} = \delta_\lambda \delta_\mu \qquad\qquad \lambda, \mu > 0 \tag{9}$$

Proof. Let us suppose that the equation 9 is correct. Therefore, considering the $\downarrow$-continuity of the δ_v at the origin, we get :

$$\delta_\lambda \leq \underset{\mu \geq \lambda}{\wedge} \delta_\mu = \underset{v>0}{\wedge} \delta_{\lambda+v} = \underset{v>0}{\wedge} \delta_v \delta_\lambda = \delta_\lambda$$

Therefore, the equation 8 of the ball $B_\lambda(x)$ is reduced to

$$B_\lambda(x) = \delta_\lambda(x) \wedge \breve{\delta}_\lambda(x)$$

As, moreover, $\{\delta_\lambda(x), x \in \mathcal{L}\}$ are symmetrical, they become identified with the balls $B_\lambda(x)$ of the infered metrics. Let then $x, y \in \mathcal{L}$ with $d(x,y) = \lambda + \mu$; from equation 9 , we get

$$y \in \delta_{\lambda+\mu}(x) = \delta_\mu \delta_\lambda(x);$$

therefore, there exists an element $z \in \mathcal{L}$ such that $z \leq \delta_\lambda(x)$ and $y \leq \delta_\mu(z)$, or, considering the triangular inequality between x, y and z such that :

$$d(x,z) + d(z,y) \leq \lambda + \mu = d(x,y) \leq d(z,y) + d(z,y).$$

Element z is exactly at the distances λ from x and μ from y. When λ and μ vary, element z describes the geodesics between x and y.

Conversely, let us suppose the existence of a geodesic from x to y, and let $y \leq \delta_{\lambda+\mu}(x)$. Let us consider an element z on this geodesic, in the ratio of the distances $\frac{\lambda}{\lambda+\mu}$ to x and $\frac{\mu}{x+\mu}$ to y. As $d(x,y) \leq \lambda + \mu$, the distance from z to x satisfies the inequality

$$d(x,z) = \frac{\lambda}{\lambda+\mu} d(x,y) \leq \lambda \qquad \text{or} \quad z \leq \delta_\lambda(x)$$

Similarly, we have $z \leq \delta_\mu(y)$, or as well $y \leq \delta_\mu(z)$, and by composition product $y \leq \delta_\mu \delta_\lambda(x)$, so that $\delta_{\lambda+\mu} \leq \delta_\lambda \delta_\mu$, which ends the proof. ■

When coming back to Choquet proposition 8, it is enough to note that, as the existence of geodesics is a stronger characteristic than a well linking of the space, dilations that satisfy the semigroup 9 enable us to extract the connected components (as soon as finite distances only are involved).

Furthermore, it is easy to notice that, when the metric lattice is *discrete*, the well linking condition is equivalent to the existence of geodesics. Therefore, in this case, the semigroup dilations 9 are the *only ones* that can extract arcwise connected components.

8 geodesics and digital connections

In the previous sections, we explored various metric structures by comparing them with *topological* connectivity (in $\mathcal{P}(\mathbb{R}^n)$) or *arcwise* connectivity (in $\mathcal{P}(\mathbb{Z}^n)$). However, in mathematical morphology, set connectivity is replaced by the wider concept of a connection on $\mathcal{P}(E)$, defined as follows [11].

Definition 10 *Given space E, we call connection on $\mathcal{P}(E)$ any class $\mathcal{C} \subseteq \mathcal{P}(E)$ that satisfies the three following axioms :*

i/ $\mathcal{C}$ contains the empty space : $\emptyset \in \mathcal{C}$

ii/ $\mathcal{C}$ contains the singletons : $x \in E \Rightarrow \{x\} \in \mathcal{C}$

iii/ the union of any family of elements of $\mathcal{C}$ with a non-empty intersection still belongs to $\mathcal{C}$: $\{A_i \in \mathcal{C}\}$, $\cap A_i \neq \emptyset \Rightarrow \cup A_i \in \mathcal{C}$

Any set $A \subseteq E$ is partitioned into its connected components, so that they turn out to be the invariants of a family $\{\gamma_x, x \in E\}$ of point connected openings, as they are called, such that for all $\{x,y\} \in E$ and any $A \subseteq E$, we have

- $\gamma_x(x) = \{x\}$
- $\gamma_x(A) = \gamma_y(A)$ *or otherwise* $\gamma_x(A) \cap \gamma_y(A) = \emptyset$
- $x \notin A \Rightarrow \gamma_x(A) = \emptyset$

Conversely, the data of a family of openings, associated to each point of E and satisfying these three properties is the characteristic of a unique connection ([11], theorem 2.8).

The connection concept is too wide to let us hope that all the previous results can be extended. For instance, given a partition $\triangle$ of E, of classes D(x), if we consider the connection

$$\mathcal{C} = \{D(x) \cap A, \quad x \in \mathbb{R}^n, \quad A \in \mathcal{P}(\mathbb{R}^n)\} \cup \emptyset$$

and the Euclidean distance, the existence of ultimate eroded points is not sure as soon as some classes D(x) are topologically open. This is the reason why we will restrict ourselves to discrete metrics, while maintaining its generality to E, and we consider uniquely those distances that map E $\otimes$ E into $\mathbb{Z}_+$.

The relationships between metrics and connection may be considered as two reciprocal formulations, depending whether it is wondered to what extend a metric induces a connection or conversely.The answer to the first question is given by the following proposition, from Ch. Ronse and J. Serra [12][10].

Proposition 11 *Let E be an arbitrary set, $\alpha : \mathcal{P}(E) \to \mathcal{P}(E)$ be an extensive and symmetrical dilation, and let $x \in E$ and $A \in \mathcal{P}(E)$. Then the limit under iteration*

$$\gamma_x(A) = \cup \left\{ (\alpha(x) \cap A)^{(n)}, \quad n > 0 \right\} \tag{10}$$

considered as an operation on A is a point connected opening.

Note that it is not necessary to provide $\mathcal{P}(E)$ with a connection beforehand. So, even disregarding any possible arcwise connectivity, dilations by unit balls of $\mathbb{R}^n$, such as square, cube, hexagon, etc ... *do generate* connections, that they use to extract the connected components afterwards. But proposition 11 goes further, as it extends this characteristic to any extensive and symmetrical dilation. "Dilation" may even be replaced with "increasing operation".

We now look into the converse question, and wonder how a given connection $\mathcal{C}$ on $\mathcal{P}(E)$ may induce a metric. Associate with every point x of E, the class $\mathcal{C}(x)$ of the connected components containing x and whose intersection with any set $A \subseteq E$ containing x is itself connected

$$\mathcal{C}(x) = \{C : x \in C \in \mathcal{C};\ x \in A \subseteq E \ \Rightarrow\ \gamma_x(A) \cap C \in \mathcal{C} \backslash \emptyset\}$$

This class is not empty, as it contains the singleton $\{x\}$. As it is obviously stable for the union, it admits a maximal element $\delta(x)$. In order to match the conditions of proposition 11, we have to make δ symmetrical, that is to say replace it with

$$\alpha(x) = \delta(x) \cap \overset{\checkmark}{\delta}(x) \quad \textit{where} \quad \overset{\checkmark}{\delta}(x) = \{y : x \in \delta(y)\}$$

As $x \in \delta(x)$, it also belongs to $\overset{\checkmark}{\delta}(x)$, and $\alpha(x)$, connected, is therefore an element of $\mathcal{C}(x)$. The equation 10, applied to the dilation by a structuring

element $\alpha(x)$ then leads to a new point opening, γ_x^* say, which characterizes a new connection $\mathcal{C}^*$. As $\alpha(x) \in \mathcal{C}(x)$, we have for any set A containing point x

$$\{x\} \subseteq [\alpha(x) \cap A]^{(n)} \subseteq A$$

therefore $\gamma_x^*(A) \subseteq \gamma_x(A)$. However, the inclusion may be strict. For instance, if we take for E the completed digital line, for $\mathcal{C}$ the arc connection, and for A a connected set containing a point at infinity, then set A remains inacessible to any marker with finite co-ordinates. To sum up, we can state the following

Proposition 12 *Any connection $\mathcal{C}$ on $\mathcal{P}(E)$, where E is an arbitrary space, induces on $\mathcal{P}(E)$ a wider extensive and symmetrical connected dilation, which, in its turn (prop. 12), generates a new connection $\mathcal{C}^*$, which is less rich than $\mathcal{C}$.*

We can see things differently, and notice that $\mathcal{C}^*$ is the experimentally accessible subset of connection $\mathcal{C}$. Besides, the components of $\mathcal{C}^*$, or of $\mathcal{C}$, happen to be reached from the first dilation step of α, when $\alpha^{(2)} = \alpha$. For instance, if we consider the above-mentionned connection, which is induced by the intersection of the classes $D(x)$ of a fixed partition $\triangle$, we find for any point $x \in E$

$$\begin{aligned} \delta(x) &= \overset{\checkmark}{\delta}(x) = \alpha(x) = D(x) = \alpha^{(n)}(x) \\ \gamma_x^*(A) &= \gamma_x(A) = A \cap D(x) \end{aligned}$$

and if two points in A are two different classes of the partition, their ecart is infinite.

9 Examples of digital geodesic metrics

From the previous sections, it is clear that the semigroup structure $\delta_\gamma \delta_\mu = \delta_{\lambda+\mu}$ is unavoidable. But fortunately, a number of families $\{\delta_\lambda\}$ can be built, that can satisfy it. Here are a few, in two or three dimensions. It is reminded that in the discrete spaces, the semigroup 9 is equal to

$$\delta_n = (\delta_1)^n$$

but that $\delta_1(x)$ can change its shape from one point to another one.

Metrics of regular lattices : those are precisely the ones where $\delta_1(x)$ shape does not change, i.e. which are translation invariant on a a regular grid, such as,

in $\mathbb{Z}^2$ the symmetrical unit square of 9 or 5 points (diamonds), or the 7 point hexagon.

in $\mathbb{Z}^3$ cube (27 points), the hexagonal basis-cylinder (21 points) or the cube-octahedron (13 points), the last one being the finest and the most isotropic.

geodesic metrics of a first mask : In practice, the previous metrics are only useful when the studied object is contained in a rectangular mask, Z say, which does not happen very often. Most of the time, on the contrary, the mask has cut out a region in a wider field, and, in order to manage this border effect, $\delta_1(x)$ is replaced by $\delta_1(x) \cap Z$. The same construction is correct when Z is an arbitrary given set, as the examples of sections 3 and 5 have shown it. Besides, iterating a first geodesic used as an initial metric, in order to build a second one, is not forbiden.

Non unit dilations : Let us consider now as a unit ball the dilate δ_n of size n of the unit isotropic dilation of the grid, i.e. the square 3 x 3, or the 13 voxels cube-octahedron, for instance. The procedure consists of changing the connection, by replacing arcwise connectivity by that of the δ_n. It means that the component containing a given point x is not a one piece object anymore, but a group of objects whose dilate by δ_n is in one piece.

This non unit geodesics may save considerable time in 3-dimensional processes. Suppose for example we want to extract the arcwise connected component A_x at point x of a given set A. We can begin by eroding A by δ_n, then reconstruct it w.r. to the unit ball δ_n, and ending the process by geodesic dilations according to the unit ball δ_1. For large diameters of A compared to n, the computing time is asymptotically divided by n.

Sections and projections : As we have seen before about the kidney branchings, the projection of the stack of sections pile projection normally to their plane may be used as a basis for a tridimensional analysis. Consider for example a 3-D set A (in $\mathbb{R}^2$or in $\mathbb{Z}^2$), of connected component $\gamma_x(A)$ at point x. Let A_0 and x_0 be the projections of A and x respectively on a horizontal plane subspace.Then the vertical cylinder of basis the connected component of A_0 (in the 2-D sense) that includes x_0 contains $\gamma_x(A)$. Such a property allows an easy extraction of $\gamma_x(A)$, specially when the connected components of A are rather well separated.Beyond projection procedures, here again, it is not difficult to find non unit dilations and the accompanying connections. But in this case, only vertically aligned points can be gathered.

The following example illustrates this projection technique.The sequence under study comprises 57 8-bit digital images of 512 x 512 pixels. They come from a bone tissue, examined by confocal microscopy, with a one micron digital spacing. In this small volume of bone, we can see three osteocytes which are located at various depths. On both slices of 16, the nuclei appear, as well as portions of long fibers of cytoplasm, that we are about to segment.

By taking the supremum of the 57 slices (17a) and filtering them, we keep the three largest projections only (17b) where the three disjoint connected projections of the osteocytes are visible. Consider the vertical cylinders with these projections as the bases, and restrict each of 57 sections to the inside of the cylinders. This results in figure18, that shows a perspective view of the extracted cells.

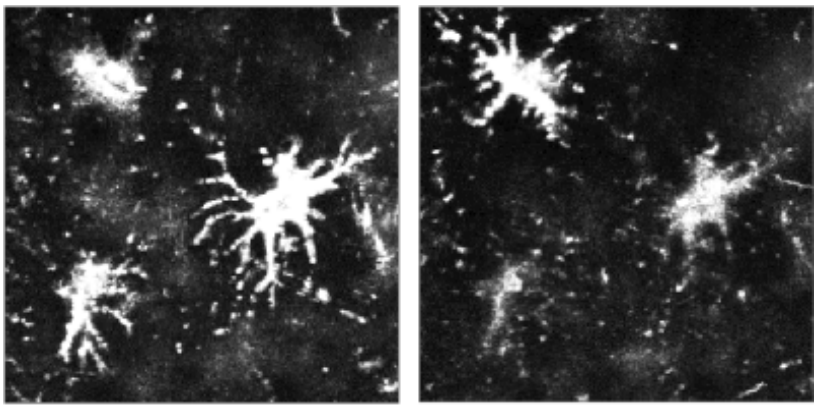

Figure 16: Sections numbers 15 (a), and 35 (b), from a stack of 57 confocal sections of osteocytes.

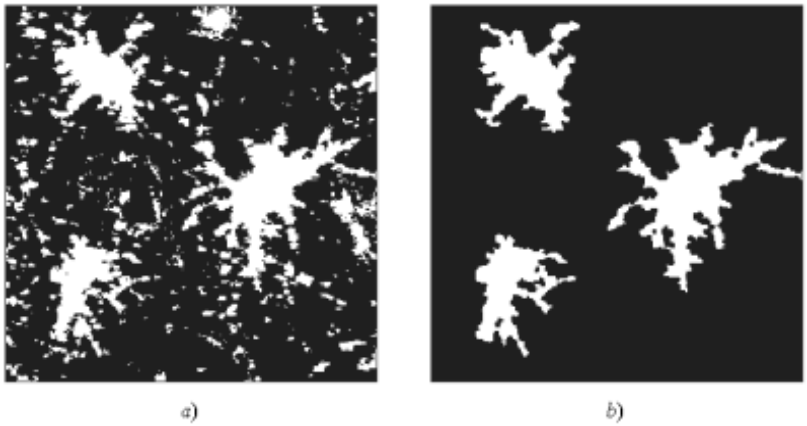

Figure 17: a) Threshold version of the supremum ; b) Extraction of the three largest objects.

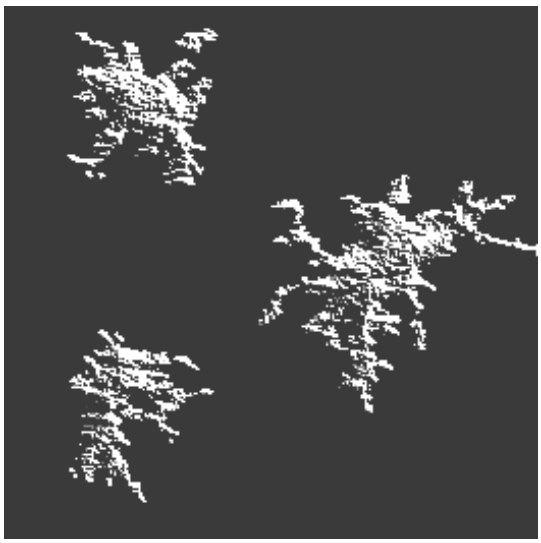

Figure 18: Perspective view of the extracted oesteocytes

In geodesic terms, these operations are equivalent to geodesic dilations by a vertical segment, taken as the unit dilating ball. This segment size is not one, but about fifteen points (otherwise, the whole cylinder could not be found). Then, only objects whose vertical dilate is arcwise-connected are considered connected, which finally yields the three largest cells of the stack.

10 Conclusion

Remarkably, the same wavefront concept in $\mathbb{R}^n$ or $\mathbb{Z}^n$ allows one to describe :
- the connected components,via its surface measurement;
- the bottlenecks, via the minima of its variation;
- the branches, via the variation of its connectivity;
- and the extremities, via through its ultimate locations;

and its application to complex 3-D histologic structures proves the outstanding power of this tool.

From a theoretical point of view, the wavefront properties bridge the three concepts of connection, metrics and dilation. An additive semi-group of dilations is equivalent to a metric that admits geodesics, as well as to the compact connected components of a connection. This double equivalence opens the door to an a-priori infinite number of possibilities ; in fact, it seems up to now that connections by dilation are the only ones to have proved their practical usefulness.

Acknowledgement 13 *On the one hand, I thank Dr J. Bertram, and Dr Staub and M. M. Mendjeli on the other hand, for the discussions we had together, and for the digital data they kindly gave me. I also thank M. Ch. Bernard for his comments about sequential monotone convergence of connected compact sets. I did not use them here, but this talk helped me in the relaunching of this writing. Finally, I thank M. G. Fricout : thanks to his different point of view about the study of kidney tress, he forced me to explain my own position more clearly.*

References

[1] Clark A.T., Young R.J. and Bertram J.F. In vitro studies on the roles of transforming growth factor-beta1 in rat metaphrenic development, *Kidney Int* 59 pp 1641-1653 (2001).

[2] Choquet G. *Topologie* Masson Paris, 1966.

[3] Fricout G. Kidney and Skeletonization Int. report CMM, *Ecole des Mines de Paris* nov 2000.

[4] Fricout G., Cullen-Mc Ewen L.A., Harper I.A., Jeulin D., Bertram J.F. A quantitative method for analysing 3D branching in embryonic kidneys: development of a technique and preliminary data. (to be presented at *ISS'*2001,Bordeaux, France sept. 2001).

[5] Hadwiger H. *Vorselungen uber Inhalt, Operflache und Isoperimetrie.* Springer, Berlin, 1957.

[6] Klein J-C. *Conception et réalisation d'une unité logique pour £'analyse quantitative d'images.* Thesis, University of Nancy, 1976.

[7] Lantuejoul C., Beucher S. On the use of the geodesic metric in image analysis. *J. of Microscopy.* Vol. 121, 1981, pp. 39-49.

[8] Matheron G. *Random Sets and Integral Geometry.*New York: Wiley, 1975.

[9] Meyer F. Rapport de stage note interne CMM, (1976).

[10] Ronse Ch., Serra J.Geodesy and connectivity in grids (to be published in *Fundamenta Informaticae*).

[11] Serra J. (ed.) *Image Analysis and Mathematical Morphology.* Vol. 2. : *Theoretical Advances.* Academic Press, London, 1988.

[12] Serra J. Connectivity on complete lattices, *J. of Math. Imaging and Vision* 9, 231-251 (1998).

[13] Serra J. Cube, cube-octahedron or rhombododecahedron as bases for 3-D shape descriptions", *Advances in Visual Form Analysis, C. Arcelli and Al. (eds.)* World Scientific 1997, 502-519.

[14] M. Staub' personnal communication.